

# An optical transistor of the nonlinear resonant structure

Jongbae Kim\*

Quantum Technology Research Division, ETRI, Daejeon 34129, Republic of Korea  
KREONET Center, KISTI, Daejeon 34141, Republic of Korea

(Dated: arXiv, January 23, 2026)

An optical transistor capable of simultaneous amplification and switching is theoretically proposed via cascaded second-order nonlinear interactions in a resonant structure. Two distinct operational schemes are analyzed. A single frequency scheme employs cascaded second harmonic generation and inverse second harmonic generation (SHG/iSHG) using two Type-I SHG interactions, whereas a dual frequency scheme employs cascaded SHG and optical parametric amplification (SHG/OPA). Exact theoretical solutions and numerical calculations show cascadable amplification and digital on/off switching. A new optical phenomenon of nonlinear transparency is predicted by the theoretical solutions and confirmed by the numerical solutions in each scheme of the cascaded SHG/iSHG and SHG/OPA. The single and dual frequency configurations satisfy the cascadability and fan-out criteria with power transfer ratios of  $\alpha_{TR} = 4.838$  and  $52.26$  and power amplification factors of  $\beta_{AF} = 48.38$  and  $522.6$ , respectively. These results indicate transistor-like performance at input powers in the milliwatt range, readily supplied by laser diodes. The proposed structure establishes a physically feasible and practically scalable route to optical transistors operating at high speed and low power for integrated photonic circuits, with broad applications in all optical communication and computing.

## I. INTRODUCTION

An optical transistor is a device that amplifies and switches optical signals simultaneously. If the optical transistor can be implemented, all optical processing will be possible in various fields of optical technologies, especially enabling the implementation of optical computing with high-speed performance beyond that of electronic computing. However, since optical waves do not interact with each other in classical linear optics due to the zero charge of a photon, which cannot be controlled by electric potential, it is difficult to control one optical wave with another for all optical processing.

Despite many difficulties, various schemes using multiple media have been proposed to implement optical transistors. These include silicon microring configuration [1], electromagnetically induced absorption using a microresonator [2], a one-dimensional photonic-crystal cavity with an active Raman gain medium [3], polariton fluids in the plane of the microcavity [4], optical control of exciton fluxes [5], tunneling of light through frustrated total internal reflection in a photonic crystal structure [6], a microcavity with a ladder-type polymer for polariton relaxation [7], deep-level defects in nitride semiconductors [8], and single-photon nonlinearity in a polymer-coupled microcavity forming exciton-polaritons [9]. Meanwhile, since the observation of SHG [10] and the theoretical establishment of the nonlinear optical interactions [11], based on the characteristics that induce direct interactions among optical waves, second-order nonlinear interactions have been applied to the research on the optical transistor. This research includes a device wherein a weak incoming signal controls a strong outgoing signal

utilizing SHG [12] and frequency-degenerate quadratic three-wave interactions in a Type-II SHG geometry [13]. However, it is still known that an optical transistor comparable to an electronic transistor has not been realized yet.

In spite of extensive efforts to realize an optical transistor using diverse media and device schemes in Refs. [1–13], a practical implementation is still elusive. An optical transistor should satisfy stringent criteria, particularly cascadability and fan-out, in order to be practically useful [14]. For comparison, an electronic transistor normally exhibits a current transfer ratio  $\alpha \simeq 0.95\text{--}0.99$  and a current amplification factor  $\beta \simeq 20\text{--}200$ , while an analogous optical device should achieve a power transfer ratio  $\alpha_{TR} \geq 2$  for the fan-out and a power amplification factor  $\beta_{AF} \approx \beta$  to be comparable to electronic transistors. Several proposals in Refs. [1–11] have demonstrated simultaneous amplification and switching; however, realizing a practical optical transistor that satisfies the demanding criteria and achieves performance truly comparable to that of an electronic transistor remains a significant challenge. Aside from the schemes in Refs. [1–11], the two approaches described in Refs. [12, 13] are based on classical second-order nonlinear equations and theoretical analysis; nevertheless, they also suffer from fundamental limitations—namely, excessively high pump requirements ( $\sim 10^6$  W or  $\sim 1$  GW/cm<sup>2</sup>), lack of a clear off state, and inability to satisfy the cascadability and the fan-out requirements—thereby hindering practical feasibility.

In contrast, the proposed optical transistor employs a nonlinear waveguide within a resonant structure as a single compact device, enabling efficient cascaded interactions, well defined digital on/off states, and operation at low input powers readily supplied by commercial laser diodes. The collector output exceeds both base and

\* jongbae@etri.re.kr; jongbae@sci.kr

emitter inputs, achieving sufficiently large  $\alpha_{TR}$  and  $\beta_{AF}$ , thereby demonstrating compliance with the cascadability and the fan-out requirements among the criteria. Moreover, the underlying cascaded SHG/iSHG and SHG/OPA processes have been theoretically analyzed and numerically verified, clarifying how physical parameters govern transistor behavior. Through these analyses, the proposed structure is shown to overcome the limitations of earlier designs and to achieve performance levels that are comparable to, and in some respects competitive with, electronic transistors.

In this paper, to address the issue of realizing an optical transistor comparable to an electronic transistor, two schemes for the optical transistor based on the second-order nonlinear interactions in the resonant structure are proposed. For each scheme, either single or dual frequency optical waves are needed for the operation. The single frequency waves interact with each other through cascaded SHG/iSHG, whereas the dual frequency waves interact with each other through cascaded SHG/OPA [15]. In the optical transistor, the base wave controls the emitter wave and in turn the collector wave, thereby implementing the simultaneous amplification and switching of the optical signals.

This paper is organized as follows. In Sec. II, for one scheme of the optical transistor operating with waves of a single frequency, a theory of two Type-I SHG interactions in the nonlinear resonant structure is proposed. Theoretical solutions of the cascaded SHG/iSHG and SHG/SHG equations are derived for the analysis of the two Type-I SHG interactions. Numerical solutions for the cascaded SHG/iSHG are calculated and plotted to demonstrate the amplification and the switching. In Sec. III, for the other scheme of the optical transistor operating with waves of dual frequencies, the cascaded SHG/OPA interactions in the nonlinear resonant structure are considered. Theoretical solutions of the cascaded SHG/OPA are derived and numerical solutions are calculated for the analysis and the illustration. Finally, implications for the optical transistor of the nonlinear resonant structure are summarized in Sec. IV.

## II. AN OPTICAL TRANSISTOR WITH WAVES OF A SINGLE FREQUENCY

### A. Theory of two Type-I SHGs

For the physical implementation of the optical transistor operating with waves of a single frequency in the nonlinear resonant structure, the second-order nonlinear interactions of the two Type-I SHGs are proposed in the present study. The two Type-I SHGs inherently involve SHG and iSHG which are indispensable for the amplification and for the switching in the optical transistor. SHG is a second-order nonlinear optical process in which a fundamental wave of identical frequency and polarization interacts within a nonlinear medium

to generate a second harmonic wave at twice the frequency ( $\omega_p + \omega_p \rightarrow \omega_h = 2\omega_p$ ). In this work, SHG is explicitly referred to as Type-I SHG to distinguish it from Type-II SHG. iSHG is an inverse phenomenon of SHG. In this process, a fundamental wave ( $\omega_s$ ) and its second harmonic wave ( $\omega_h$ ) interact with a nonlinear material, and their mixing leads to amplification of the fundamental wave ( $\omega_h - \omega_s \rightarrow \omega_s = \omega_h - \omega_s$ ). The proposed SHG/iSHG interactions are the cascaded processes of SHG  $\omega_p + \omega_p \rightarrow \omega_h = 2\omega_p$  and iSHG  $\omega_h - \omega_s \rightarrow \omega_s = \omega_h - \omega_s$  in the second-order nonlinear optical phenomena. In these phenomena, each of a pump wave and a signal wave is independently coupled to a single second harmonic wave without direct coupling between the two of the pump and the signal wave. The second harmonic wave generated in the SHG interaction resonates inside the structure and serves as a source in iSHG.

In Fig. 1, a schematic diagram for the optical transistor operating with waves of a single frequency in the nonlinear resonant structure is shown. A waveguide with a nonlinear susceptibility  $\chi^{(2)}$  and an interaction length  $L$  is placed between two mirrors with reflection and transmission coefficients  $r_1$ ,  $t_1$ ,  $r_2$ , and  $t_2$  for the second harmonic wave. The pump wave and the signal wave are incident on mirror 1 and the amplified signal wave is transmitted through mirror 2, but the second harmonic wave is singly resonant between the two mirrors in the structure.

In the scheme, if the pump wave from the emitter is first incident solely on mirror 1 and passes through the nonlinear waveguide, the second harmonic wave is generated. The second harmonic wave resonates inside the structure composed of the mirrors with  $r_1 = r_2 = 100\%$  [16] and increases its power through the SHG interaction with the pump wave. Then the power of the incident pump wave can be adjusted so that the entire pump wave is depleted and converted into the second harmonic wave. The output power of the optical waves exiting the collector in this case is null and can be defined to be zero, indicating a digital off state. Subsequently, the signal wave can be prepared, which has the same frequency but orthogonal polarization compared with the pump wave. If the signal wave from the base is sequentially incident on the mirror 1 and passes through the nonlinear waveguide, the signal wave interacts with the resonant second harmonic wave so as to generate an idler wave by way of the iSHG interaction. Since the pump wave frequency is equal to the signal wave frequency, the frequencies of the pump wave, the signal wave, and the idler wave are identical. The idler wave emerging from the collector in this case is the amplified signal wave whose output power is not zero and can be defined to be one, indicating a digital on state. It is assumed in the meantime that the two mirrors in the resonant structure reflect the second harmonic wave exclusively, but transmit all other waves including the pump and the signal wave. In this way, the base wave controls the emitter wave so that the collector wave is manipulated for amplification and for switching.

In a nonlinear resonant structure, both a resonant wave and single pass waves can mix and give rise to nonlinear interactions. If the number of resonant cycles,  $n$ , of a resonant wave is introduced into the nonlinear equations describing interactions among single pass waves, then the single pass equations with the wave amplitudes indexed by  $n$  can in general describe the nonlinear interactions among a resonant wave and single pass waves. Thus, the interaction among a resonant second harmonic wave and

other single pass waves can be simplified to the interaction among a single pass second harmonic wave and other single pass waves at a general stage in the resonant cycle  $n$  [17].

On the basis of the SHG equations and the resonant structure formalism [11, 17], the governing equations for the two Type-I SHGs, proposed to describe the cascaded SHG/iSHG interactions in the  $n$ -th resonant cycle, can be represented as

$$\partial_z E_{p,n}(z) = -\frac{\alpha_p}{2} E_{p,n}(z) + i \frac{2\omega_p}{n_p c N_p} \kappa_p^{SHG} E_{p,n}^*(z) E_{h,n}(z) e^{i\Delta\beta_p^{SHG} z}, \quad (1a)$$

$$\partial_z E_{s,n}(z) = -\frac{\alpha_s}{2} E_{s,n}(z) + i \frac{2\omega_s}{n_s c N_s} \kappa_s^{SHG} E_{s,n}^*(z) E_{h,n}(z) e^{i\Delta\beta_s^{SHG} z}, \quad (1b)$$

$$\begin{aligned} \partial_z E_{h,n}(z) = & -\frac{\alpha_h}{2} E_{h,n}(z) + i \frac{2\omega_h}{n_h c N_h} \frac{\kappa_{hp}^{SHG}}{2} E_{p,n}^2(z) e^{-i\Delta\beta_p^{SHG} z} \\ & + i \frac{2\omega_h}{n_h c N_h} \frac{\kappa_{hs}^{SHG}}{2} E_{s,n}^2(z) e^{-i\Delta\beta_s^{SHG} z}, \end{aligned} \quad (1c)$$

under the slowly varying envelope approximation. Here  $E_{i,n}(z)$ ,  $\kappa_i^{SHG}$ ,  $\alpha_i$ ,  $\omega_i$ ,  $N_i$ , and  $n_i$  ( $i=p$ ,  $s$ ,  $h$ ,  $hp$ , or  $hs$ ) denote a complex amplitude of an electric field defined as  $\vec{E}_{i,n}(\vec{x}, t) = \vec{E}_{i,n}(x, y) E_{i,n}(z) e^{i(\beta_i z - \omega_i t)} + c.c.$  from a real classical electric field, a nonlinear coupling constant defined as  $\kappa_p^{SHG} = \int dx dy \vec{E}_p^*(x, y) \frac{\chi^{(2)}}{2} \vec{E}_h(x, y) \vec{E}_p^*(x, y)$  etc., a propagation loss constant, an angular frequency, a normalization constant of integration defined as  $N_i = \int dx dy |\vec{E}_{i,n}(x, y)|^2$ , and an effective index of refraction corresponding to the pump wave, the signal wave, and the second harmonic wave, respectively. The phase factors  $\Delta\beta_p^{SHG} = \beta_h - 2\beta_p - \beta_\Lambda$  and  $\Delta\beta_s^{SHG} = \beta_h - 2\beta_s - \beta_\Lambda$  are the SHG phase mismatches among the propagation constants  $\beta_i = \frac{\omega_i}{c} n_i(\omega_i, \hat{e}_i)$  and  $\beta_\Lambda = \frac{2\pi N}{\Lambda}$ . Here  $\hat{e}_i$ ,  $\Lambda$ ,  $N$ , and  $c$  denote the polarization unit vector, the period of quasi phase matching, the positive integer of a phase matching order, and the speed of light in vacuum, respectively. The propagation modes in the waveguide are determined from the decoupled wave equation  $(\partial_x^2 + \partial_y^2 + \omega_i^2 \mu_0 \epsilon - \beta_i^2) \vec{E}_{i,n}(x, y) = 0$ , implying that the solution  $\vec{E}_{i,n}(x, y)$  is independent of the number  $n$  in the function. The nonlinear equations in Eqs. (1) are symmetric with respect to  $p \leftrightarrow s$  interchange and possess the two Type-I SHGs that can potentially contain both SHG and iSHG in themselves.

## B. Theoretical analysis

For a theoretical study of the nonlinear equations in Eqs. (1), the phase matching condition  $\Delta\beta_p^{SHG} = \Delta\beta_s^{SHG} = 0$  is implicitly imposed on the nonlinear optical processes to be discussed below. In particular, in the two Type-I SHGs, the phase matching requires a wave-

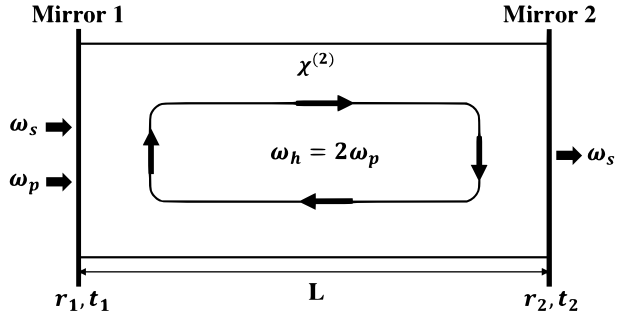


FIG. 1. A schematic diagram for the optical transistor operating with the waves of the single frequency in the nonlinear resonant structure.

uide condition

$$n_p(\omega_p, \hat{e}_p) = n_s(\omega_s, \hat{e}_s) \quad (2)$$

for the two effective indices of refraction of the pump wave and the signal wave that possess the same frequency  $\omega_p = \omega_s$  but orthogonal polarizations  $\hat{e}_p \cdot \hat{e}_s = \delta_{p,s}$ . While uniaxial crystals such as LiNbO<sub>3</sub> intrinsically possess identical bulk refractive indices along two orthogonal axes, achieving the condition in Eq. (2) may constitute the most demanding challenge in realizing a waveguide cavity with very low loss for the practical implementation of the present optical transistor based on the nonlinear resonant structure.

In the lossless limit  $\alpha_i = 0$  for analytical convenience, the complex equations in Eqs. (1) can be written again in terms of real equations to be solved for exact theoretical solutions. To this end, the complex amplitudes of the

electric fields can be first represented as

$$E_{p,n}(z) = \sqrt{\frac{\omega_p}{n_p c N_p}} u_{p,n}(z) e^{i\phi_{p,n}(z)}, \quad (3a)$$

$$E_{s,n}(z) = \sqrt{\frac{\omega_s}{n_s c N_s}} u_{s,n}(z) e^{i\phi_{s,n}(z)}, \quad (3b)$$

$$E_{h,n}(z) = \sqrt{\frac{\omega_h}{2n_h c N_h}} u_{h,n}(z) e^{i\phi_{h,n}(z)}, \quad (3c)$$

and the nonlinear coupling constants can be replaced by

$$K_p = 2\kappa_p \frac{\omega_p}{n_p c N_p} \sqrt{\frac{\omega_h}{2n_h c N_h}}, \quad (4a)$$

$$K_s = 2\kappa_s \frac{\omega_s}{n_s c N_s} \sqrt{\frac{\omega_h}{2n_h c N_h}}. \quad (4b)$$

For the expressions in Eqs. (4), the nonlinear coupling constants are defined as  $\kappa_p^{SHG} = \kappa_p e^{i\delta_p}$ ,  $\kappa_s^{SHG} = \kappa_s e^{i\delta_s}$  and Kleinman symmetry [18] is used for the relations  $\kappa_p^{SHG} = \kappa_{hp}^{SHG*}$ ,  $\kappa_s^{SHG} = \kappa_{hs}^{SHG*}$ . Also, two parameters for the nonlinear phase difference can be defined as

$$\theta_{p,n}(z) = \phi_{h,n}(z) - 2\phi_{p,n}(z) + \delta_p, \quad (5a)$$

$$\theta_{s,n}(z) = \phi_{h,n}(z) - 2\phi_{s,n}(z) + \delta_s, \quad (5b)$$

to handle the phases of the complex electric fields and the nonlinear coupling constants.

Taking all of these into consideration, the nonlinear equations of the two Type-I SHGs in Eqs. (1) can be expressed as

$$\partial_z u_{p,n}(z) = -K_p u_{p,n}(z) u_{h,n}(z) \sin \theta_{p,n}(z), \quad (6a)$$

$$\partial_z u_{s,n}(z) = -K_s u_{s,n}(z) u_{h,n}(z) \sin \theta_{s,n}(z), \quad (6b)$$

$$\begin{aligned} \partial_z u_{h,n}(z) &= K_p u_{p,n}^2(z) \sin \theta_{p,n}(z) \\ &+ K_s u_{s,n}^2(z) \sin \theta_{s,n}(z), \end{aligned} \quad (6c)$$

$$\partial_z \theta_{p,n}(z) = \frac{\Gamma_n(z)}{u_{h,n}^2(z)} + 2 \frac{\cos \theta_{p,n}(z)}{\sin \theta_{p,n}(z)} \partial_z \ln u_{p,n}(z), \quad (6d)$$

$$\partial_z \theta_{s,n}(z) = \frac{\Gamma_n(z)}{u_{h,n}^2(z)} + 2 \frac{\cos \theta_{s,n}(z)}{\sin \theta_{s,n}(z)} \partial_z \ln u_{s,n}(z). \quad (6e)$$

For the sake of notational simplicity in Eqs. (6d)–(6e) and for later discussion, an additional definition of a parameter  $\Gamma_n(z)$  is introduced as

$$\begin{aligned} \Gamma_n(z) &= K_p u_{p,n}^2(z) u_{h,n}(z) \cos \theta_{p,n}(z) \\ &+ K_s u_{s,n}^2(z) u_{h,n}(z) \cos \theta_{s,n}(z). \end{aligned} \quad (7)$$

The real equations in Eqs. (6) are the complete equivalence of the complex equations in Eqs. (1). The real equations show that the amplitudes of the pump wave and the signal wave still remain decoupled from each other but coupled to the second harmonic wave, while the parameters of the nonlinear phase difference corresponding to the two waves are coupled with each other in the presence of  $\Gamma_n(z)$ .

Then, from Eqs. (6), conserved quantities for the two Type-I SHGs in the general  $n$ -th resonant cycle can be derived for further analysis. For the first constant of integration, the Manley–Rowe relation [19] can be derived, leading to

$$\sum_i^{p,s,h} u_{i,n}^2(z) = \sum_i^{p,s,h} u_{i,n}^2(0) \quad (8)$$

from Eqs. (6a)–(6c). The relation in Eq. (8) is the conservation of total power flow in the waveguide with the power expression  $P_{i,n}(z) = 2\epsilon_0 n_i c N_i |E_{i,n}(z)|^2$ . As for the second constant of integration, the parameter  $\Gamma_n(z)$  is an intrinsically conserved quantity, given by

$$\partial_z \Gamma_n(z) = 0, \quad (9)$$

which can be derived from Eqs. (6d)–(6e). For the conserved quantity  $\Gamma_n(z)$ , if  $K_p \rightarrow 0$  or  $K_s \rightarrow 0$ ,  $\Gamma_n(z)$  reduces to the well known constant of integration for a single Type-I SHG in single pass propagation. An additional third constant of integration can be derived from Eqs. (6a)–(6b) as

$$\frac{\partial_z \ln u_{p,n}(z)}{\partial_z \ln u_{s,n}(z)} = \frac{K_p}{K_s} \cdot \frac{\sin \theta_{p,n}(z)}{\sin \theta_{s,n}(z)}. \quad (10)$$

The constancy of the relation in Eq. (10) will be discussed in the next section.

### C. Solutions of cascaded SHG/iSHG

The nonlinear equations in Eqs. (6) are essentially combined forms of two SHG equations for the pump wave and the signal wave in the absence of any direct coupling between the amplitudes of the two waves. The equations involve five unknown parameters—three amplitudes and two nonlinear phase differences to be solved. Nevertheless, the second constant of integration in Eq. (9) provides the solutions for the two parameters of the nonlinear phase differences in Eqs. (6d)–(6e), which in turn can be used to solve the three amplitude equations in Eqs. (6a)–(6c).

If the pump wave is initially incident alone on the emitter and passes through the nonlinear waveguide, the initial condition for the second harmonic wave is

$$u_{h,0}(0) = 0 \quad (11)$$

in the beginning of the SHG interaction and resonance. This condition implies that  $\Gamma_0(z) = 0$  and then  $\cos \theta_{p,0}(z) = 0$ . Since the backward propagation of the second harmonic wave from  $z = L$  to  $z = 0$  does not change the nonlinear phases, it follows that  $\cos \theta_{p,1}(0) = 0$ , so that  $\Gamma_1(z) = 0$  and hence  $\cos \theta_{p,1}(z) = 0$ . This process can be applied to repeat during the resonance, increasing the number of resonant cycles in consecutive order, to finally obtain  $\cos \theta_{p,n}(z) = 0$  in the  $n$ -th cycle.

In addition, the second harmonic wave is assumed to be resonating under the resonant feedback [20, 21] and the backward propagation condition [17]

$$E_{h,n+1}(0) = r_1 r_2 e^{-\frac{\alpha_h}{2} L} e^{2i\beta_h L} E_{h,n}(L) \quad (12)$$

where the resonant wave itself participates in the nonlinear interactions in each feedback. If the pump wave is followed by the signal wave, the nonlinear phase of the second harmonic wave is still preserved in the presence of the signal wave as well. Even if the pump wave and the signal wave are incident at the same time, the process is identical to the case as explained just above. Therefore, the absence of the initial input for the second harmonic wave in Eq. (11) leads to

$$\Gamma_n(z) = 0 \quad (13)$$

and thus  $\cos \theta_{p,n}(z) = \cos \theta_{s,n}(z) = 0$ , because the condition in Eq. (13) is maintained for any arbitrary values of  $K_i$  and  $u_{i,n}(z)$  ( $i = p, s, h$ ). Consequently, the second constant of integration provides

$$\theta_{p,n}(z) = \pm \frac{\pi}{2}, \quad \theta_{s,n}(z) = \pm \frac{\pi}{2} \quad (14)$$

which are also the solutions of Eqs. (6d)–(6e). The nonlinear phase differences are constant and conserved without the loss of generality in the resonance. Then the first constant of integration in Eq. (8) and the third constant of integration in Eq. (10) can be used to obtain the solution for the remaining one amplitude parameter.

Now, the exact theoretical solutions of the nonlinear equations in Eqs. (6) can be obtained in the following two cases. In the first scheme, if  $\kappa_p = -\kappa_s$  with  $\sin \theta_{p,n}(0) = \sin \theta_{s,n}(0)$ , the third constant of integration in Eq. (10) reduces to

$$\frac{\partial_z \ln u_{p,n}(z)}{\partial_z \ln u_{s,n}(z)} = -1 \quad (15)$$

and gives a relation between the amplitudes of the pump wave and the signal wave as

$$u_{s,n}(z) = u_{s,n}(0) \frac{u_{p,n}(0)}{u_{p,n}(z)}. \quad (16)$$

The relation in Eq. (16) shows that the amplitude of the signal wave is inversely proportional to the amplitude of the pump wave. Therefore, it explicitly indicates that the signal wave can be amplified if the pump wave is deamplified. Along with the relations from the three constants of integration, after some algebra, analytical solutions of the cascaded SHG/iSHG can be obtained from Eqs. (6a)–(6c) as

$$u_{p,n}(z) = \frac{U_n(0)}{\sqrt{2}\sqrt{1+k_n^2}} [\text{dn}\{b(z+z_n), k_n\} + k_n \text{cn}\{b(z+z_n), k_n\}], \quad (17a)$$

$$u_{s,n}(z) = \frac{U_n(0)}{\sqrt{2}\sqrt{1+k_n^2}} [\text{dn}\{b(z+z_n), k_n\} - k_n \text{cn}\{b(z+z_n), k_n\}], \quad (17b)$$

$$u_{h,n}(z) = \frac{\sqrt{2}k_n U_n(0)}{\sqrt{1+k_n^2}} \text{sn}[b(z+z_n), k_n]. \quad (17c)$$

Here, the expressions  $\text{sn}(z, k)$ ,  $\text{cn}(z, k)$ ,  $\text{dn}(z, k)$ , and  $\text{sc}(z, k)$  in Eq. (21) below stand for Jacobi elliptic functions [22, 23].

For the simplification of the solutions, four constants  $U_n(0)$ ,  $k_n$ ,  $b$ , and  $z_n$  are introduced in the expressions. The constant  $U_n(0)$ , which can be written as

$$U_n(0) = \sqrt{u_{p,n}^2(0) + u_{s,n}^2(0) + u_{h,n}^2(0)}, \quad (18)$$

plays the role of the amplitude in each Jacobi elliptic function in the solutions. The modulus  $k_n$ , which can be defined as

$$k_n^2 = \frac{U_n^2(0) - 2u_{p,n}(0)u_{s,n}(0)}{U_n^2(0) + 2u_{p,n}(0)u_{s,n}(0)} \quad (19)$$

with  $0 \leq k_n \leq 1$ , determines the characteristics of the

Jacobi elliptic functions and the parameter  $b$  can be represented as

$$b = \frac{\sqrt{2}K_p \sin \theta_{p,n}(0)U_n(0)}{\sqrt{1+k_n^2}}. \quad (20)$$

The spatial displacement  $z_n$  in the presence of  $u_{h,n}(0)$  in the  $n$ -th resonant cycle can be given by

$$z_n = \frac{1}{b} \text{sc}^{-1} \left[ \frac{u_{h,n}(0)}{u_{p,n}(0) - u_{s,n}(0)}, k_n \right] \quad (21)$$

in the present scheme. With all of the parameters, the expressions in Eq. (14) and Eqs. (17) are the exact solutions for the cascaded SHG/iSHG with  $K_p = -K_s$  in Eqs. (6). From the point of view concerned with the behaviors of the Jacobi elliptic functions, the solutions suggest that, in the range  $0 \leq z \leq L$  of the nonlinear

resonant structure, the pump wave should be deamplified due to the summation of the functions  $dn(z,k)$  and  $cn(z,k)$ , while the signal wave should be amplified due to the difference between the functions  $dn(z,k)$  and  $cn(z,k)$ .

In the limit as  $k_n \rightarrow 0$  in the solutions, a condition

$$u_{p,n}(0) = u_{s,n}(0), \quad u_{h,n}(0) = 0 \quad (22)$$

is derived from Eqs. (18)–(19), and in this case, the condition leads to the solutions

$$u_{i,n}(z) = u_{i,n}(0), \quad (i = p, s, h) \quad (23)$$

from Eqs. (17). The solutions in Eq. (23) show a phenomenon of nonlinear transparency that illustrates the transparent propagation of the pump wave and the signal wave without the nonlinear interactions in the waveguide. The nonlinear transparency is due to the balance and the equilibrium between SHG and iSHG as can be proved from Eqs. (6a)–(6c). The SHG/iSHG transparency can be confirmed, as well, by the numerical calculations of the complex equations in Eqs. (1) with the initial conditions of the three waves, for example  $P_{p,n}(0) = P_{s,n}(0) = 10$  mW,  $P_{h,n}(0) = 0$ , as required by Eq. (22). It can be used for a verification of the waveguide condition in Eq. (2) with or without a resonant structure under the present consideration. In the limit as  $k_n \rightarrow 1$ , Eqs. (17) reduce to the solutions of a single Type-I SHG driven by the pump wave with  $u_{s,n}(z) = 0$  which implies a condition  $u_{s,n}(0) = 0$  imposed by Eq. (19).

Numerical solutions in the scheme of  $\kappa_p = -\kappa_s$  can be obtained from the direct calculations of the complex equations in Eqs. (1) with  $\kappa_p^{SHG} = -\kappa_s^{SHG}$  under the condition in Eq. (12). These types of solutions can include behaviors of solutions of the nonlinear equations where the signs of the nonlinear coupling constants are opposite such as  $\kappa_p^{SHG} \cdot \kappa_s^{SHG} < 0$ . For the convenience of numerical calculations, it is assumed that  $\kappa_p^{SHG}/N_p = \kappa_{hp}^{SHG}/N_h = d_{21} \cdot \eta_{eff}$ ,  $\kappa_s^{SHG}/N_s = \kappa_{hs}^{SHG}/N_h = d_{22} \cdot \eta_{eff}$ , and the signal wave sequentially follows the pump wave that is first incident alone to generate the resonant second harmonic wave. Here  $d_{21}$  and  $d_{22}$  stand for the elements of the d-coefficient matrix and  $\eta_{eff}$  is the effective mode factor including the overlap integral of waves. Then the pump wave polarized along the X-axis and the signal wave polarized along the Y-axis are coupled with the second harmonic wave polarized along the Y-axis, where X, Y, and Z are the principal coordinate axes in the crystal frame. For the calculations of solutions and the plotting, physical parameters  $-d_{21} = d_{22} = 3$  pm/V,  $\eta_{eff} = 0.9$ ,  $\alpha_h = 3\alpha_p = 0.003$  dB/cm, wavelengths  $\lambda_p = \lambda_s = 1550$  nm for  $\omega_p = \omega_s$ ,  $n_p = n_s = 2.1544$ ,  $n_h = 2.2325$ , and  $L = 4$  cm are adopted. Together with the inputs  $P_{p,n}(0) = 10$  mW,  $P_{s,n}(0) = 1$  mW,  $N_i = 1 \mu\text{m}^2$ , and  $n = 100$ , the power of the two waves  $P_{p,s}(z)$  from the solutions is plotted as a function of waveguide coordinate  $z$  in the laboratory frame in Fig. 2, including the factor  $\frac{2}{\pi}$  from quasi-phase matching. Here,  $N_i = 1 \mu\text{m}^2$  is assumed only for analytical convenience; the present formalism is not restricted to this

cross-sectional area and applies equally to general optical waveguides with arbitrary  $N_i$ . The notation  $P_{p,s}(z)$  denotes the plotted power traces of the pump and signal, i.e.,  $P_{p,s}(z) \equiv \{P_{p,n}(z), P_{s,n}(z)\}$ . The deamplification of the pump wave due to SHG that can define the digital off state and the amplification of the signal wave due to iSHG that can define the digital on state are demonstrated in the figure. The numerical solutions of Eqs. (1) constitute an independent confirmation of the behaviors of the analytical solutions in Eqs. (17).

Regarding input power limits, the operational power limits are determined primarily by the properties of the reflection mirrors and the waveguide. The SiN semiconductor DBRs and the LiNbO<sub>3</sub> crystal waveguide are promising candidates as they exhibit high optical damage thresholds. Representative reported values for LiNbO<sub>3</sub> crystal waveguides include 26 MW/cm<sup>2</sup> [24],  $2.36 \times 10^5$  W/cm<sup>2</sup> [25], and 300–500 MW/cm<sup>2</sup> in recent commercial products [26]. These reported thresholds are sufficient to sustain the resonant wave power calculated in this work, namely  $P_{h,n}(L)/P_{p,n}(0) \simeq 69.1$  for  $L = 4$  cm in the cascaded SHG/iSHG scheme and  $P_{h,n}(L)/P_{p,n}(0) \simeq 53.7$  for  $L = 1$  cm to be discussed later in the cascaded SHG/OPA scheme.

There is no widely accepted definition of efficiency for optical transistors yet. However, the power transfer ratio and the power amplification factor can serve as appropriate figures of merit to represent the efficiency of the proposed device. Similar to the characteristics of an electronic transistor, in the optical transistor of the present study the power transfer ratio  $\alpha_{TR}$  can be defined as

$$\alpha_{TR} = \frac{P_{s,n}(L)}{P_{p,n}(0)} \quad (24)$$

to represent the ratio of the output power of the signal wave out of the collector to the input power of the pump wave incident on the emitter. Likewise, the power amplification factor  $\beta_{AF}$  can be defined as

$$\beta_{AF} = \frac{P_{s,n}(L)}{P_{s,n}(0)} \quad (25)$$

to represent the ratio of the output power of the signal wave out of the collector to the input power of the signal wave incident on the base. From the numerical results of the collector power  $P_{s,n}(L) = 48.38$  mW, the power transfer ratio  $\alpha_{TR} = 4.838$  and the power amplification factor  $\beta_{AF} = 48.38$  can be obtained in the present calculations.

Although the waveguide length  $L = 4$  cm, as indicated by the numerical analysis above and as shown in Fig. 2, may appear long for practical applications, more compact form factors can be achieved through several approaches. Among these, artificial enhancement of  $d_{21}$  and  $d_{22}$  during the growth of LiNbO<sub>3</sub> constitutes an essential approach, as it directly strengthens the nonlinear interaction underlying the transistor operation. Alternatively, the use of materials possessing intrinsically larger nonlin-

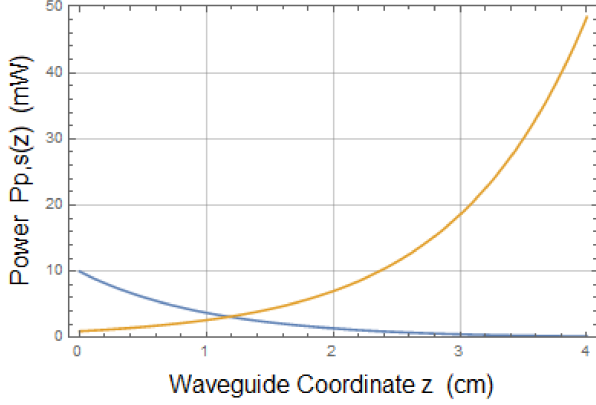


FIG. 2. The blue curve shows the deamplification of the pump wave due to SHG, while the yellow curve shows the amplification of the signal wave due to iSHG.

ear coefficients would also enable shorter devices. In addition, the use of a switching deadband enables a broader definition of the digital off state, thereby making shorter lengths feasible. Regarding the switching deadband, the deadband width  $\Delta P = P_{\text{on}} - P_{\text{off}}$  can serve as a useful figure of merit. As one example, in the present device this reduces to  $\Delta P = P_{p,n}(0) - P_{p,n}(0)/2 = P_{p,n}(0)/2$ , which scales directly with the input pump power. For instance,  $\Delta P = 5$  mW when  $P_{p,n}(0) = 10$  mW and  $\Delta P = 0.5$  mW when  $P_{p,n}(0) = 1$  mW. Therefore, if the off state is defined below  $P_{\text{off}} = P_{p,n}(0)/2 = 5$  mW for the sole input of the pump wave, practical operation can be realized with  $L \geq 1$  cm, because the output collector power is calculated to be  $P_{p,n}(L) = 8.1643, 4.9502, 1.3737, 0.391, 0.124, 0.0433$  mW for  $L = 0.5, 1.0, 2.0, 3.0, 4.0, 5.0$  cm, respectively. The input signal power can then be independently chosen so that the power transfer ratio  $\alpha_{TR} = P_{s,n}(L)/P_{p,n}(0) \geq 2$ , thereby satisfying the fan-out criterion. Design modifications to the waveguide that increase the effective mode factor as  $\eta_{\text{eff}} \rightarrow 1$  will also help shorten the waveguide toward a compact form. These considerations indicate that the proposed structure, though initially demonstrated with  $L = 4$  cm, can be realistically adapted to more compact dimensions through parameter optimizations and material choices.

#### D. Solutions of cascaded SHG/SHG

In the second scheme, if  $\kappa_p = \kappa_s$  with  $\sin \theta_{p,n}(0) = \sin \theta_{s,n}(0)$ , the third constant of integration in Eq. (10) reduces to

$$\frac{\partial_z \ln u_{p,n}(z)}{\partial_z \ln u_{s,n}(z)} = 1 \quad (26)$$

and gives a relation between the amplitudes of the pump wave and the signal wave expressed as

$$u_{s,n}(z) = u_{s,n}(0) \frac{u_{p,n}(z)}{u_{p,n}(0)}. \quad (27)$$

The relation in Eq. (27) shows that the signal wave amplitude is linearly proportional to the pump wave amplitude. Therefore, it explicitly indicates that the signal wave can be deamplified if the pump wave is deamplified. After some algebra similar to the first scheme, analytical solutions of the cascaded SHG/SHG can be obtained from Eqs. (6a)–(6c) as

$$u_{p,n}(z) = \frac{u_{p,n}(0)U_n(0)\text{cn}[b(z + z_n), k_n = 1]}{\sqrt{u_{p,n}^2(0) + u_{s,n}^2(0)}}, \quad (28a)$$

$$u_{s,n}(z) = \frac{u_{s,n}(0)U_n(0)\text{cn}[b(z + z_n), k_n = 1]}{\sqrt{u_{p,n}^2(0) + u_{s,n}^2(0)}}, \quad (28b)$$

$$u_{h,n}(z) = U_n(0)\text{sn}[b(z + z_n), k_n = 1]. \quad (28c)$$

Here, two constants  $U_n(0)$  and  $b$  are adopted from the expressions in Eq. (18) and Eq. (20), respectively. The spatial displacement  $z_n$  can be given as

$$z_n = \frac{1}{b} \sinh^{-1} \left[ \frac{u_{h,n}(0)}{\sqrt{u_{p,n}^2(0) + u_{s,n}^2(0)}} \right] \quad (29)$$

in the present scheme. The expressions in Eq. (14) and Eqs. (28) are the exact solutions for the cascaded SHG/SHG with  $K_p = K_s$  in Eqs. (6). The solutions in Eqs. (28) include two SHG interactions for the simultaneous deamplifications of the pump wave and the signal wave with only the inherent  $k_n = 1$ . In the limit  $u_{p,n}(0) \rightarrow 0$  or  $u_{s,n}(0) \rightarrow 0$ , Eqs. (28) reduce to the well known solutions of a single Type-I SHG interaction.

Numerical solutions in the scheme of  $\kappa_p = \kappa_s$  can be obtained from the direct calculations of the complex equations in Eqs. (1) with  $\kappa_p^{\text{SHG}} = \kappa_s^{\text{SHG}}$  and the condition in Eq. (12). These types of solutions can include behaviors of solutions of the nonlinear equations where the signs of the nonlinear coupling constants are identical such as  $\kappa_p^{\text{SHG}} \cdot \kappa_s^{\text{SHG}} > 0$ . Before the calculations, let us first consider the relationship between the two  $\kappa_p = -\kappa_s$  and  $\kappa_p = \kappa_s$  cases in the nonlinear equations. In the case of  $\kappa_p^{\text{SHG}} = \pm \kappa_s^{\text{SHG}}$ , the two sets of the complex equations can be related by the amplitude transformation of the signal wave

$$E_{s,n}(z) \rightarrow \pm i E_{s,n}(z) \quad (30)$$

in Eqs. (1), or equivalently, the corresponding sets of the real equations with  $K_p = \pm K_s$  can be related by the nonlinear phase transformation of the signal wave

$$\phi_{s,n}(z) \rightarrow \phi_{s,n}(z) \pm \frac{\pi}{2} \quad (31)$$

in Eqs. (6). This means that, in the two schemes with the nonlinear coupling constants mentioned above, the

two sets of the nonlinear equations for the cascaded SHG/iSHG and the cascaded SHG/SHG can be transformed from one to the other by means of the transformation in Eq. (30) or Eq. (31). However, the implications of Eq. (5b), Eqs. (6), and Eq. (13) suggest that the nonlinear phase shift of the signal wave  $\phi_{s,n}(0) \rightarrow \phi_{s,n}(0) \pm \frac{\pi}{2}$  at the initial input should lead to the same effect as Eq. (31) and consequently, the initial amplitude change  $E_{s,n}(0) \rightarrow \pm iE_{s,n}(0)$  in Eqs. (1) leads to the same effect as Eq. (30). Therefore, the numerical solutions for the deamplification of the pump wave and the amplification of the signal wave can be obtained from the cascaded SHG/SHG equations with  $\kappa_p^{SHG} = \kappa_s^{SHG}$  and equivalently, the numerical solutions for the simultaneous deamplifications of the pump and the signal wave can be obtained from the cascaded SHG/iSHG equations with  $\kappa_p^{SHG} = -\kappa_s^{SHG}$  as well.

For the numerical solutions of Eqs. (1) with  $\kappa_p^{SHG} = \kappa_s^{SHG}$  to include the deamplification of the pump wave and the amplification of the signal wave, all the parameters in the  $\kappa_p^{SHG} = -\kappa_s^{SHG}$  calculations are used as they are, but  $d_{21} = d_{22} = 3 \text{ pm/V}$  and  $P_{s,n}(0) = 1 \text{ mW}$  with the phase-shifted amplitude  $e^{\pm i\frac{\pi}{2}}E_{s,n}(0)$  are adopted. As discussed in Eq. (30), the numerical solutions in this  $\kappa_p^{SHG} = \kappa_s^{SHG}$  case show that they are consistent with the numerical solutions in the  $\kappa_p^{SHG} = -\kappa_s^{SHG}$  case and provide the same graph as in Fig. 2. In the same manner as discussed above, the numerical solutions for simultaneous yet independent deamplifications of the pump wave and the signal wave can be demonstrated in Eqs. (1) with  $\kappa_p^{SHG} = -\kappa_s^{SHG}$  and the  $\pm \frac{\pi}{2}$  phase shift of the signal input amplitude, as well as with  $\kappa_p^{SHG} = \kappa_s^{SHG}$  and the zero phase shift of the initial input amplitudes. The solutions in these two cases are also consistent with each other.

In a typical second-order nonlinear material like LiNbO<sub>3</sub> to implement the optical transistor as discussed in this section, the second-order nonlinear coefficient  $d_{26} = 0$ . This means that there is no interaction caused by a direct coupling among the three waves participating in the Type-I SHG/iSHG interactions through  $d_{21}$  and  $d_{22}$  with the second harmonic wave of Y-polarization. Since the second-order nonlinear coefficient  $d_{16} \neq 0$  in general, however, the three waves can simultaneously participate in the Type-II SHG interaction through  $d_{16}$  with the second harmonic wave of X-polarization. In this context, Type-II SHG is a second-order nonlinear optical process in which two fundamental waves of identical frequency ( $\omega_p = \omega_s$ ) but orthogonal polarization ( $\hat{e}_p \cdot \hat{e}_s = 0$ ) interact within a nonlinear material to generate a second harmonic wave at twice the frequency ( $\omega_p + \omega_s \rightarrow \omega_h = \omega_p + \omega_s$ ). The generation of the second harmonic wave due to  $d_{16}$  reduces the amplification of

the signal wave. If the SHG interaction is carried out by way of the sole pump wave before the signal wave input, the power of the second harmonic wave resonating with Y-polarization is much stronger than the power of the pump wave input such as  $P_{h,n}(0)/P_{p,n}(0) \simeq 66.5$  in the numerical calculations of Fig. 2. Thus the power of the signal wave in the presence of  $d_{16} (= d_{21} = -d_{22})$  relative to the power of the signal wave in the absence of  $d_{16}$  is not much reduced to  $P_{s,n}^{d_{16}=d_{21}}(L)/P_{s,n}^{d_{16}=0}(L) = 98.7\%$  in the present calculations. Hence even in the presence of  $d_{16}$ , an overall strong amplification of the signal wave is anticipated because the amplification degree of the signal wave due to the Type-I SHG/iSHG interactions is still greater than the deamplification degree of the signal wave due to the Type-II SHG interaction. If possible in an artificial way, it would be best to make  $d_{16} = 0$  during the growth process of a nonlinear material such as LiNbO<sub>3</sub> to avoid the Type-II SHG interaction.

### III. AN OPTICAL TRANSISTOR WITH WAVES OF DUAL FREQUENCIES

#### A. Theory of cascaded SHG/OPA

In this section, a distinct type of optical transistor employing waves of dual frequencies through cascaded SHG and OPA processes is introduced. For the physical implementation of the optical transistor operating with waves of dual frequencies in the nonlinear resonant structure, the second-order nonlinear interactions of SHG and OPA are needed for amplification and switching. In this context, OPA is a second-order nonlinear optical process in which two waves of different frequencies ( $\omega_h$  and  $\omega_s$ ) interact within a nonlinear medium, resulting in amplification of the fundamental wave ( $\omega_s$ ) and the generation of a new idler wave ( $\omega_c$ ) at the difference frequency ( $\omega_h - \omega_s \rightarrow \omega_c = \omega_h - \omega_s$ ). The cascaded SHG/OPA interactions are the processes of SHG  $\omega_p + \omega_p \rightarrow \omega_h = 2\omega_p$  and OPA  $\omega_h - \omega_s \rightarrow \omega_c = \omega_h - \omega_s$  in the second-order nonlinear phenomena. In Fig. 3, a schematic diagram for the optical transistor operating with the waves of the dual frequencies is illustrated. The nonlinear resonant structure in Fig. 3 is the same as the one in Fig. 1, but in the present scheme, a converted idler wave is generated to come out of the collector along with the signal wave. Since the pump wave frequency is different from the signal wave frequency,  $\omega_p \neq \omega_s$ , the frequencies of the pump, the signal, and the idler waves are distinguishable. For the descriptions of the cascaded SHG/OPA interactions in the n-th resonant cycle, the governing equations in the waveguide [11, 15, 17] can be represented as

$$\partial_z E_{p,n}(z) = -\frac{\alpha_p}{2} E_{p,n}(z) + i \frac{2\omega_p}{n_p c N_p} \kappa_p^{SHG} E_{p,n}^*(z) E_{h,n}(z) e^{i\Delta\beta^{SHG} z}, \quad (32a)$$

$$\begin{aligned} \partial_z E_{h,n}(z) = & -\frac{\alpha_h}{2} E_{h,n}(z) + i \frac{2\omega_h}{n_h c N_h} \frac{\kappa_h^{SHG}}{2} E_{p,n}^2(z) e^{-i\Delta\beta^{SHG} z} \\ & + i \frac{2\omega_h}{n_h c N_h} \kappa_h^{OPA} E_{s,n}(z) E_{c,n}(z) e^{-i\Delta\beta^{OPA} z}, \end{aligned} \quad (32b)$$

$$\partial_z E_{s,n}(z) = -\frac{\alpha_s}{2} E_{s,n}(z) + i \frac{2\omega_s}{n_s c N_s} \kappa_s^{OPA} E_{c,n}^*(z) E_{h,n}(z) e^{i\Delta\beta^{OPA} z}, \quad (32c)$$

$$\partial_z E_{c,n}(z) = -\frac{\alpha_c}{2} E_{c,n}(z) + i \frac{2\omega_c}{n_c c N_c} \kappa_c^{OPA} E_{s,n}^*(z) E_{h,n}(z) e^{i\Delta\beta^{OPA} z}, \quad (32d)$$

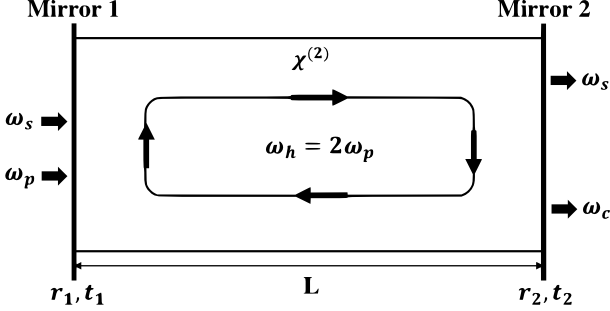


FIG. 3. A schematic diagram for the optical transistor operating with the waves of the dual frequencies in the nonlinear resonant structure.

in the slowly varying envelope approximation. All the physical parameters are defined in the same way as in Eqs. (1), but here the relevant fields are the pump, the second harmonic, the signal, and the converted idler wave. The phase factors  $\Delta\beta^{SHG} = \beta_h - 2\beta_p - \beta_\Lambda$ ,  $\Delta\beta^{OPA} = \beta_h - \beta_s - \beta_c - \beta_\Lambda$  are the phase mismatches of SHG and OPA, while the relations  $\kappa_p^{SHG} = \kappa_h^{SHG*}$ ,  $\kappa_s^{OPA} = \kappa_c^{OPA} = \kappa_h^{OPA*}$  can be adopted from the Kleinman symmetry.

## B. Theoretical analysis

For a theoretical study of cascaded SHG/OPA described in Eqs. (32), the analytical procedures similar to those used in the previous schemes of the two Type-I SHGs are employed. In the lossless limit,  $\alpha_i = 0$ , the complex equations in Eqs. (32) can be formulated again in terms of real equations to obtain exact theoretical solutions. Along with the complex amplitudes of the electric fields in Eqs. (3) and

$$E_{c,n}(z) = \sqrt{\frac{\omega_c}{n_c c N_c}} u_{c,n}(z) e^{i\phi_{c,n}(z)}, \quad (33)$$

the nonlinear coupling constants can be replaced by

$$K_a = 2\kappa_a \sqrt{\frac{\omega_s}{n_s c N_s}} \sqrt{\frac{\omega_c}{n_c c N_c}} \sqrt{\frac{\omega_h}{2n_h c N_h}} \quad (34)$$

and  $K_p$  in Eq. (4a). For the expressions in Eq. (34), the nonlinear coupling constants are defined as  $\kappa_s^{OPA} = \kappa_a e^{i\delta_a}$  and the relation  $\kappa_s^{OPA} = \kappa_c^{OPA} = \kappa_h^{OPA*}$  is used. Also, another parameter for the nonlinear phase difference is defined as

$$\theta_{a,n}(z) = \phi_{h,n}(z) - \phi_{s,n}(z) - \phi_{c,n}(z) + \delta_a \quad (35)$$

to deal with the phases of the complex electric fields and the nonlinear coupling constants. With all these considerations, the nonlinear equations of the cascaded SHG/OPA in Eqs. (32) can be expressed as

$$\partial_z u_{p,n}(z) = -K_p u_{p,n}(z) u_{h,n}(z) \sin \theta_{p,n}(z), \quad (36a)$$

$$\partial_z u_{s,n}(z) = -K_a u_{s,n}(z) u_{h,n}(z) \sin \theta_{a,n}(z), \quad (36b)$$

$$\partial_z u_{c,n}(z) = -K_a u_{c,n}(z) u_{h,n}(z) \sin \theta_{a,n}(z), \quad (36c)$$

$$\begin{aligned} \partial_z u_{h,n}(z) = & K_p u_{p,n}^2(z) \sin \theta_{p,n}(z) \\ & + 2K_a u_{s,n}(z) u_{c,n}(z) \sin \theta_{a,n}(z), \end{aligned} \quad (36d)$$

$$\partial_z \theta_{p,n}(z) = \frac{\Gamma_n(z)}{u_{h,n}^2(z)} + 2 \frac{\cos \theta_{p,n}(z)}{\sin \theta_{p,n}(z)} \partial_z \ln u_{p,n}(z), \quad (36e)$$

$$\begin{aligned} \partial_z \theta_{a,n}(z) = & \frac{\Gamma_n(z)}{u_{h,n}^2(z)} + \frac{\cos \theta_{a,n}(z)}{\sin \theta_{a,n}(z)} \partial_z \ln u_{s,n}(z) \\ & + \frac{\cos \theta_{a,n}(z)}{\sin \theta_{a,n}(z)} \partial_z \ln u_{c,n}(z). \end{aligned} \quad (36f)$$

For the expressions of Eqs. (36e)–(36f), an additional parameter  $\Gamma_n(z)$  is defined as

$$\begin{aligned} \Gamma_n(z) = & K_p u_{p,n}^2(z) u_{h,n}(z) \cos \theta_{p,n}(z) \\ & + 2K_a u_{s,n}(z) u_{c,n}(z) u_{h,n}(z) \cos \theta_{a,n}(z) \end{aligned} \quad (37)$$

in the present scheme. The real equations in Eqs. (36) are the exact equivalents of the complex equations in Eqs. (32). The real equations show that the amplitudes of the signal wave and the converted idler wave are mutually interchanged so as to couple to the second harmonic wave in the corresponding equations, while the parameters of the nonlinear phase difference are coupled with each other in the presence of  $\Gamma_n(z)$ .

Then from the nonlinear equations in Eqs. (36), conserved quantities can be derived for each resonant cycle  $n$ .

For the first two constants of integration, Manley–Rowe relations can be derived as

$$\sum_i^{p,s,c,h} u_{i,n}^2(z) = \sum_i^{p,s,c,h} u_{i,n}^2(0), \quad (38a)$$

$$u_{s,n}^2(z) - u_{c,n}^2(z) = u_{s,n}^2(0) - u_{c,n}^2(0), \quad (38b)$$

from Eqs. (36a)–(36d) and these relations result in the conservation of total power flow in the waveguide. As for the second constant of integration, the parameter  $\Gamma_n(z)$  is an intrinsically conserved quantity expressed as

$$\partial_z \Gamma_n(z) = 0 \quad (39)$$

that can be derived from Eqs. (36e)–(36f). In the case of the conserved quantity  $\Gamma_n(z)$ , if  $K_p \rightarrow 0$  or  $K_a \rightarrow 0$ ,  $\Gamma_n(z)$  reduces to the well known constant of integration for a single Type-I SHG or OPA in the single pass propagation. The other two constants of integration, which relate the amplitudes of the pump, signal, and idler waves, can be derived from Eqs. (36a)–(36c) and expressed as

$$\frac{\partial_z \ln[u_{s,n}(z) + u_{c,n}(z)]}{\partial_z \ln u_{p,n}(z)} = \frac{K_a}{K_p} \cdot \frac{\sin \theta_{a,n}(z)}{\sin \theta_{p,n}(z)}, \quad (40a)$$

$$\frac{\partial_z \ln[u_{s,n}(z) - u_{c,n}(z)]}{\partial_z \ln u_{p,n}(z)} = -\frac{K_a}{K_p} \cdot \frac{\sin \theta_{a,n}(z)}{\sin \theta_{p,n}(z)}, \quad (40b)$$

where the constancy of the relations in Eqs. (40) is the same as that discussed in Sec. II. These relations are associated with the amplitude coupling among the three waves and will later be found, in Eqs. (43), to exhibit a correspondence with the Manley–Rowe relation in Eq. (38b).

### C. Solutions of cascaded SHG/OPA

The nonlinear equations in Eqs. (36) are the cascaded processes of Type-I SHG and OPA for the pump, the signal, and the converted idler wave. The equations involve six parameters for the four amplitudes and the two nonlinear phase differences to be solved. The second constant of integration in Eq. (39) provides the solutions

for the two parameters of the nonlinear phase difference in Eqs. (36e)–(36f) which in turn can be used to solve the four equations in Eqs. (36a)–(36d). As discussed in Sec. II, the absence of the initial input for the second harmonic wave in Eq. (11) leads to  $\Gamma_n(z) = 0$  in the present cascaded SHG/OPA as well. Consequently, the solutions of the nonlinear equations in Eqs. (36e)–(36f) are

$$\theta_{p,n}(z) = \pm \frac{\pi}{2}, \quad \theta_{a,n}(z) = \pm \frac{\pi}{2} \quad (41)$$

from  $\cos \theta_{p,n}(z) = \cos \theta_{a,n}(z) = 0$ . The nonlinear phase differences are constant and conserved in the nonlinear resonant structure.

In the present scheme, if  $K_p = K_a$  is assumed with  $\sin \theta_{p,n}(0) = -\sin \theta_{a,n}(0)$  and under the approximations  $1 - \omega_s \omega_c / \omega_p^2 = (\Delta\omega)^2 / \omega_p^2 \ll 1$ ,  $1 - n_s n_c / n_p^2 = (\Delta n)^2 / n_p^2 \ll 1$ , then the third constants of integration in Eqs. (40) reduce to

$$\frac{\partial_z \ln[u_{s,n}(z) + u_{c,n}(z)]}{\partial_z \ln u_{p,n}(z)} = -1, \quad (42a)$$

$$\frac{\partial_z \ln[u_{s,n}(z) - u_{c,n}(z)]}{\partial_z \ln u_{p,n}(z)} = 1, \quad (42b)$$

and yield relations among the amplitudes of the pump, signal, and idler waves as shown below

$$u_{s,n}(z) + u_{c,n}(z) = [u_{s,n}(0) + u_{c,n}(0)] \frac{u_{p,n}(0)}{u_{p,n}(z)}, \quad (43a)$$

$$u_{s,n}(z) - u_{c,n}(z) = [u_{s,n}(0) - u_{c,n}(0)] \frac{u_{p,n}(z)}{u_{p,n}(0)}. \quad (43b)$$

The relations in Eqs. (43) show that the summation of the amplitudes of the signal wave and the idler wave is inversely proportional to the pump wave amplitude, while the difference between the two amplitudes is linearly proportional to the pump wave amplitude. Therefore the relations indicate that, if the pump wave is deamplified, the signal wave and the idler wave can be co-amplified whereas the difference between the two amplitudes can be reduced.

After some algebra similar to that used in the schemes in Sec. II, analytical solutions of the cascaded SHG/OPA processes can be obtained from Eqs. (36a)–(36d) as

$$u_{p,n}(z) = \frac{U_n(0)}{\sqrt{2}V_n(0)\sqrt{1+k_n^2}}[\text{dn}\{b(z+z_n), k_n\} + k_n \text{cn}\{b(z+z_n), k_n\}], \quad (44a)$$

$$\begin{aligned} u_{s,n}(z) &= \frac{1}{2} \frac{U_n(0)}{\sqrt{1+k_n^2}} [\text{dn}\{b(z+z_n), k_n\} - k_n \text{cn}\{b(z+z_n), k_n\}] \\ &+ \frac{1}{2} \frac{\sqrt{V_n^2(0)-1}}{V_n(0)} \frac{U_n(0)}{\sqrt{1+k_n^2}} [\text{dn}\{b(z+z_n), k_n\} + k_n \text{cn}\{b(z+z_n), k_n\}], \end{aligned} \quad (44b)$$

$$\begin{aligned} u_{c,n}(z) &= \frac{1}{2} \frac{U_n(0)}{\sqrt{1+k_n^2}} [\text{dn}\{b(z+z_n), k_n\} - k_n \text{cn}\{b(z+z_n), k_n\}] \\ &- \frac{1}{2} \frac{\sqrt{V_n^2(0)-1}}{V_n(0)} \frac{U_n(0)}{\sqrt{1+k_n^2}} [\text{dn}\{b(z+z_n), k_n\} + k_n \text{cn}\{b(z+z_n), k_n\}], \end{aligned} \quad (44c)$$

$$u_{h,n}(z) = \frac{\sqrt{2}k_n U_n(0)}{\sqrt{1+k_n^2}} \text{sn}[b(z+z_n), k_n]. \quad (44d)$$

For the simplified expressions of the solutions, six constants  $U_n(0)$ ,  $V_n(0)$ ,  $W_n(0)$ ,  $k_n$ ,  $b$ , and  $z_n$  are introduced. The expressions for the three constants  $U_n(0)$ ,  $V_n(0)$ , and  $W_n(0)$  relevant to the amplitudes can be determined from

$$U_n^2(0) = u_{p,n}^2(0) + u_{s,n}^2(0) + u_{c,n}^2(0) + u_{h,n}^2(0), \quad (45a)$$

$$V_n^2(0) = 1 + \frac{1}{2} \frac{[u_{s,n}(0) - u_{c,n}(0)]^2}{u_{p,n}^2(0)}, \quad (45b)$$

$$W_n^2(0) = \frac{1}{2} u_{p,n}^2(0) [u_{s,n}(0) + u_{c,n}(0)]^2, \quad (45c)$$

and the parameters  $k_n$ ,  $b$ , and  $z_n$  can be defined as

$$k_n^2 = \frac{U_n^2(0) - 2V_n(0)W_n(0)}{U_n^2(0) + 2V_n(0)W_n(0)}, \quad (46)$$

$$b = \frac{\sqrt{2}K_p \sin \theta_{p,n}(0) U_n(0)}{\sqrt{1+k_n^2}}, \quad (47)$$

$$z_n = \frac{1}{b} \text{sc}^{-1} \left[ \frac{\sqrt{2}u_{h,n}(0)}{\sqrt{2}V_n(0)u_{p,n}(0) - u_{s,n}(0) - u_{c,n}(0)} \right], \quad (48)$$

in the present scheme. The representations in Eq. (41) and Eqs. (44) are the exact solutions for the cascaded SHG/OPA with  $K_p = K_a$  in Eqs. (36). The solutions in Eqs. (44) include the cascaded SHG/OPA interactions that lead to the simultaneous amplification of the signal wave and the idler wave in the range  $0 \leq z \leq L$  of the nonlinear resonant structure.

In the limit as  $k_n \rightarrow 0$  in the solutions, a condition

$$u_{p,n}^2(0) = 2u_{s,n}(0)u_{c,n}(0), \quad u_{h,n}(0) = 0 \quad (49)$$

is derived from Eqs. (45)–(46) and under this limit, the condition leads to the solutions

$$u_{i,n}(z) = u_{i,n}(0), \quad (i = p, s, c, h) \quad (50)$$

from Eqs. (44). The solutions in Eq. (50) show the phenomenon of nonlinear transparency that illustrates

the independent transparent propagation of the pump, the signal, and the idler waves without the nonlinear interactions arising from the balance and the equilibrium established between SHG and OPA. The SHG/OPA transparency can be demonstrated analytically from Eqs. (36a)–(36d) and can also be confirmed from the numerical calculations of the complex equations in Eqs. (32) with the initial conditions of the four waves, for example  $P_{p,n}(0) = 10$  mW,  $P_{s,n}(0) = P_{c,n}(0) = 5$  mW, and  $P_{h,n}(0) = 0$ , as required in Eq. (49). In the limit as  $k_n \rightarrow 1$ , a condition  $u_{s,n}(0) + u_{c,n}(0) = 0$  is derived from Eq. (46) and the solutions in Eqs. (44) reduce to

$$u_{p,n}(z) = \frac{u_{p,n}(0)U_n(0)\text{sech}[b(z+z_n)]}{\sqrt{u_{p,n}^2(0) + u_{s,n}^2(0) + u_{c,n}^2(0)}}, \quad (51a)$$

$$u_{s,n}(z) = \frac{u_{s,n}(0)U_n(0)\text{sech}[b(z+z_n)]}{\sqrt{u_{p,n}^2(0) + u_{s,n}^2(0) + u_{c,n}^2(0)}}, \quad (51b)$$

$$u_{c,n}(z) = \frac{u_{c,n}(0)U_n(0)\text{sech}[b(z+z_n)]}{\sqrt{u_{p,n}^2(0) + u_{s,n}^2(0) + u_{c,n}^2(0)}}, \quad (51c)$$

$$u_{h,n}(z) = U_n(0)\tanh[b(z+z_n)]. \quad (51d)$$

The solutions in Eqs. (51) include SHG and sum frequency generation for the amplification of the second harmonic wave via the deamplifications of the pump, the signal, and the idler waves. In the limit  $u_{p,n}(0) \rightarrow 0$  or  $u_{s,n}(0)$ ,  $u_{c,n}(0) \rightarrow 0$ , the solutions reduce to the well known solutions of the corresponding nonlinear interactions in the case of  $k_n = 1$ .

Numerical solutions in the scheme of the cascaded SHG/OPA can be provided from the direct calculations of Eqs. (32) under the condition in Eq. (12). For the convenience of calculations, let us assume that the nonlinear coupling constant for the cascaded SHG/OPA is  $d_{33}$  and the Type-0 quasi-phase matching. All the parameters in the cascaded SHG/iSHG calculations are used but  $d_{33} = 30$  pm/V,  $\alpha_h = 3\alpha_p = 0.03$  dB/cm,  $\lambda_s = 1551$  nm, and  $L = 1$  cm are adopted. Together with the input  $P_{c,n}(0) = 0$ , the power of the three waves  $P_{p,s,c}(z)$

from the solutions is plotted as a function of the waveguide coordinate  $z$  in Fig. 4 on a dBm scale. In the linear scale version of Fig. 4, the signal and idler traces are not visually distinguishable due to both the nearly equal gain of the two waves and the chosen plotting scale. This nearly equal gain is a well known property of OPA that follows directly from the Manley–Rowe relation in Eq. (38b). Moreover, because the amplified peak powers of both waves reach  $\sim 250$  mW while their difference remains nearly constant at  $\sim 1$  mW (set by the initial conditions), the linear y-axis scale causes the two traces to overlap.

The deamplification of the pump wave due to SHG that defines the digital off state and the amplification of the signal and the idler wave due to OPA that defines the digital on state are demonstrated in the figure. From the numerical results of the collector power  $P_{s,n}(L) + P_{c,n}(L) = 522.6$  mW, the power transfer ratio  $\alpha_{TR} = 52.26$  and the power amplification factor  $\beta_{AF} = 522.6$  can be obtained. When compared with the results of the cascaded SHG/iSHG, the waveguide with the large nonlinear coupling constant and the small propagation loss constant [27] is necessary for the implementation of the efficient optical transistor. For a waveguide of length  $L$ , the response time of the present device can be defined as the propagation time of the signal wave through the resonator,

$$\Delta t_{\text{res}} = \frac{n_s}{c} \cdot L \quad (52)$$

which, for  $n_s = 2.1544$  and  $L = 1$  cm, yields  $\Delta t_{\text{res}} \simeq 71.9$  ps, much shorter than the reported response time of LiNbO<sub>3</sub> optical switches ( $< 10$  ns) [28].

For comparison with the reports in Refs. [1–13], in the single frequency configuration with  $-d_{21} = d_{22} = 3$  pm/V and  $\alpha_h = 3\alpha_p = 0.003$  dB/cm, the performance reaches  $\alpha_{TR} = 4.838$  and  $\beta_{AF} = 48.38$ , whereas in the dual frequency configuration with  $d_{33} = 30$  pm/V and  $\alpha_h = 3\alpha_p = 0.03$  dB/cm, the corresponding values increase to  $\alpha_{TR} = 52.26$  and  $\beta_{AF} = 522.6$ . These results highlight the specific performance improvements of the present structure compared to existing models, while also clarifying the relative merits and limitations between the single and dual frequency implementations. With respect to sensitivity analyses, the nonlinear coefficient  $d_{il}$  and the propagation loss constant  $\alpha_i$  are dominant factors and thus can serve as useful figures of merit. Variations in these parameters lead to significant changes in  $\alpha_{TR}$  and  $\beta_{AF}$ , thereby influencing the performance of the optical transistor, as discussed in the representative cases. To enhance  $\alpha_{TR}$  and  $\beta_{AF}$  in the single frequency transistor, it is indispensable to increase the nonlinear coefficients  $d_{21}$  and  $d_{22}$ , which constitutes an intrinsic limitation to be overcome through materials research.

The proposed optical transistor is expected to serve as a key optical device for amplifiers, switches, logic gates, and integrated circuits, with broad applications in all optical signal processing, particularly in commun-

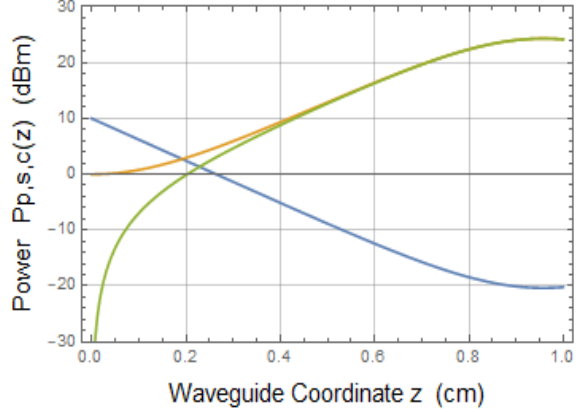


FIG. 4. The blue curve shows the deamplification of the pump wave due to SHG, while the yellow and green curves show the amplification of the signal wave and the generation of the idler wave due to OPA, respectively. All curves are plotted on a dBm scale.

cation and computing. It offers the potential for high-speed operation while maintaining low power consumption, thereby addressing the performance limitations of conventional electronic transistors. The present device can also be applied to other frequency regimes, such as the terahertz range, provided that a nonlinear resonant structure with comparable properties can be realized. As for future research, the proposed optical transistor is timely for experimental realization, as suitable materials and technologies are already available and supported by a solid theoretical foundation. A Fabry–Perot microcavity platform may appear to be a promising candidate; for example, a thin-film lithium-niobate-on-insulator microcavity based on a strip-loaded waveguide and distributed Bragg reflector mirrors in Ref. [16] may require only periodic poling for the dual frequency design, whereas the single frequency design would additionally require advances in waveguide technology.

#### IV. CONCLUSIONS

The present study theoretically establishes an optical transistor based on cascaded second-order nonlinear interactions within a resonant waveguide structure. Two representative schemes are analyzed: the cascaded SHG/iSHG scheme operating with waves of a single frequency and the cascaded SHG/OPA scheme operating with dual frequencies. When only the emitter wave is incident, its second harmonic wave is generated and resonates inside the structure, resulting in the off state of the collector output. When the base wave is applied together with the emitter wave, the collector wave appears in the on state, so that the base wave controls the emitter wave to manipulate amplification and on–off switching of the collector output. Exact theoretical solutions supported

by numerical calculations reveal that both schemes realize transistor-like operation characterized by simultaneous amplification and switching that define the digital on/off states. In both schemes, the phenomenon of nonlinear transparency is theoretically predicted and numerically confirmed, illustrating the transparent propagation of the input waves in the absence of nonlinear coupling.

In the single frequency configuration, cascaded SHG/iSHG enables cascadable signal amplification and satisfies the fan-out criterion with moderate power requirements. In the dual frequency configuration, cascaded SHG/OPA achieves substantially higher amplification and transfer efficiency because of the intrinsically larger nonlinear coefficient of LiNbO<sub>3</sub>. Both configurations satisfy the fundamental criteria for optical transistor operation, including cascadability and fan-out, confirming their functional viability. Furthermore, the achieved metrics of power transfer ratio and power amplification factor indicate performance levels comparable to

those of electronic transistors. The theoretical framework developed in this work provides a consistent formulation for describing the fundamental operating principles of optical transistors based on a nonlinear resonant structure. These findings demonstrate that an all optical transistor can be realized as a single compact device operating at high speed and low power consumption, suggesting its applicability in integrated photonic circuits for optical communication and computing.

## ACKNOWLEDGMENTS

This work was supported by projects under Grant Nos. ETRI 25ZS1200, K25L5M1C1, and by the Professional Experienced Personnel Invitation Program (2024-1-0149), all funded by the MSIT of Korea.

---

[1] L. T. Varghese, L. Fan, J. Wang, F. Gan, X. Wang, J. C. Wirth, B. Niu, C. Tansarawiput, Y. Xuan, A. M. Weiner, and M. Qi, A silicon optical transistor, *Front Opt.* (2012).

[2] B. D. Clader and S. M. Hendrickson, Microresonator-based all-optical transistor, *J. Opt. Soc. Am. B* **30**, 1329 (2013).

[3] V. G. Arkhipkin and S. A. Myslivets, All-optical transistor using a photonic-crystal cavity with an active Raman gain medium, *Phys. Rev. A* **88**, 033847 (2013).

[4] D. Ballarini, M. D. Giorgi, E. Cancellieri, R. Houdre, E. Giacobino, R. Cingolani, A. Bramati, G. Gigli, and D. Sanvitto, All-optical polariton transistor, *Nat. Commu.* **4**, 1778 (2013).

[5] P. Andreakou, S. V. Poltavtsev, J. R. Leonard, E. V. Calman, M. Remeika, Y. Y. Kuznetsova, L. V. Butov, J. Wilkes, M. Hanson, and A. C. Gossard, Optically controlled excitonic transistor, *Appl. Phys. Lett.* **104**, 091101 (2014).

[6] A. Goodarzi and M. Ghanaatshoar, Coherent all-optical transistor based on frustrated total internal reflection, *Sci. Rep.* **8**, 5069 (2018).

[7] A. V. Zasedatelev, A. V. Baranikov, D. Urbonas, F. Scafirimuto, U. Scherf, T. Stöferle, R. F. Mahrt, and P. G. Lagoudakis, A room-temperature organic polariton transistor, *Nature Photonics* **13**, 378 (2019).

[8] M. Matys, A. Domanowska, A. Michalewicz, B. Adamowicz, and T. Kachi, All-optical transistor using deep-level defects in nitride semiconductors for room temperature optical computing, *AIP Advances* **10**, 105232 (2020).

[9] A. V. Zasedatelev, A. V. Baranikov, D. Sannikov, D. Urbonas, F. Scafirimuto, V. Y. Shishkov, E. S. Andrianov, Y. E. Lozovik, U. Scherf, T. Stöferle, R. F. Mahrt, and P. G. Lagoudakis, Single-photon nonlinearity at room temperature, *Nature* **597**, 493 (2021).

[10] P. A. Franken, A. E. Hill, C. W. Peters, and G. Weinreich, Generation of optical harmonics, *Phys. Rev. Lett.* **7**, 118 (1961).

[11] J. A. Armstrong, N. Bloembergen, J. Ducuing, and P. S. Pershan, Interactions between light waves in a nonlinear dielectric, *Phys. Rev.* **127**, 1918 (1962).

[12] K. Jain and G. W. P. Jr., Optical transistor, *Appl. Phys. Lett.* **28**, 719 (1976).

[13] S. Kim, Z. Wang, D. J. Hagan, E. W. V. Stryland, A. Kobyakov, F. Lederer, and G. Assanto, Phase-insensitive all-optical transistors based on second-order nonlinearities, *IEEE J. Quantum Electron.* **34**, 666 (1998).

[14] D. A. B. Miller, Are optical transistors the logical next step?, *Nature Photonics* **4**, 1 (2010).

[15] K. Gallo, G. Assanto, and S. Stegeman, Efficient wavelength shifting over the erbium amplifier bandwidth via cascaded second order processes in lithium niobate waveguides, *Appl. Phys. Lett.* **71**, 1020 (1997).

[16] M. V. Kotlyar, S. Iadanza, and L. O'Faolain, Lithium niobate Fabry-Perot microcavity based on strip loaded waveguides, *Photonics Nanostruct.: Fundam. Appl.* **43**, 100886 (2021).

[17] J. Kim, Determination of the optimum resonance length leading to the global maximum intensity of a wave in a resonator, *J. Korean Phys. Soc.* **58**, 1591 (2011).

[18] D. A. Kleinmann, Nonlinear dielectric polarization in optical media, *Phys. Rev.* **126**, 1977 (1962).

[19] J. M. Manley and H. E. Rowe, General energy relations in nonlinear reactances, *Proc. IRE.* **47**, 2115 (1959).

[20] A. Ashkin, G. D. Boyd, and J. M. Dziedzic, Resonant optical second harmonic generation and mixing, *IEEE J. Quantum Electron.* **2**, 109 (1966).

[21] M. Fujimura, T. Suhara, and H. Nishihara, Theoretical analysis of resonant waveguide optical second harmonic generation devices, *J. Lightwave Technol.* **14**, 1899 (1996).

[22] C. G. J. Jacobi, *New Foundations of the Theory of Elliptic Functions* (Konigsberg, Borntraeger, 1829).

[23] W. A. Schwalm, *Lectures on Selected Topics in Mathematical Physics: Elliptic Functions and Elliptic Integrals* (Morgan & Claypool Publishers, 2015).

[24] S. Chen, H. Liu, Y. Kong, Z. Huang, J. Xu, and

G. Zhang, The resistance against optical damage of near-stoichiometric  $\text{LiNbO}_3:\text{Mg}$  crystals prepared by vapor transport equilibration, *Optical Materials* **29**, 885 (2007).

[25] T. Tian, T. Wu, J. Zhang, S. Wang, H. Liu, Y. Chen, Y. Chu, H. Shen, and J. Xu, Improvement of the photorefractive responsive time and optical damage resistance of  $\text{LiNbO}_3$  by co-doping with uranium and magnesium, *Optical Materials* **157**, 116223 (2024).

[26] Inrad Optics, INRAD Lithium Niobate ( $\text{LiNbO}_3$ ) Datasheet, <https://www.inradoptics.com>, accessed 8 September 2025.

[27] A. Shams-Ansari, G. Huang, L. He, Z. Li, J. Holzgrafe, M. Jankowski, M. Churaev, P. Kharel, R. Cheng, D. Zhu, N. Sinclair, B. Desiatov, M. Zhang, T. J. Kippenberg, and M. Lončar, Reduced material loss in thin-film lithium niobate waveguides, *APL Photon.* **7**, 081301 (2022).

[28] Y. Kuratani and M. Kadota, High-speed and low driving voltage  $\text{LiNbO}_3$  optical switch composed of new structure, *CLEO/QELS 2010 OSA Technical Digest*, JThE73 (2010).